

# SYNTHESIS AND CHARACTERIZATION OF TRANSITION METAL-BASED DYES FOR THE APPLICATION IN DYE SENSITIZED SOLAR CELLS

Dissertation

zur Erlangung des akademischen Grades des Doktors der  
Naturwissenschaften (Dr. rer. nat.)

eingereicht im Fachbereich Biologie, Chemie, Pharmazie  
der Freien Universität Berlin

vorgelegt von

Katja Neuthe  
aus Neubrandenburg

März 2014



Diese Arbeit wurde im Arbeitskreis von Prof. Dr. Rainer Haag im Zeitraum von Mai 2009 bis November 2014 am Institut für Chemie und Biochemie der Freien Universität Berlin angefertigt

1. Gutachter: Prof.Dr. Rainer Haag

2. Gutachter: Dr, Christoph Tzschucke

Disputation am \_\_\_06.05.2014\_\_\_\_\_



# Danksagung

Mein Dank gilt meinen Freunden, meiner Familie und meinen Arbeitskollegen.

Als erstes möchte ich mich bei Prof. Dr. Rainer Haag für die Möglichkeit bedanken dieses interessante Thema in seiner Arbeitsgruppe bearbeiten zu dürfen. Ich bedanke mich außerdem bei Dr. Carl Christoph Tzschucke für seine Beratung und Hilfe während der Doktorarbeit und für die Übernahme des Zweitgutachtens. Einen großen Dank auch an meine Freunde im Labor und Büro, insbesondere Emanuel Fleige, Dr. Aileen Justies, Nina Hoffmann, Tobias Becherer, Karolina Schaletzki, Maike Lukowiak, Lukas Artner und Olaf Wagner für die hilfreichen Ratschläge und offenen Ohren.

Den Serviceabteilungen des Instituts danke ich für ihre unverzichtbare Arbeit bei der Charakterisierung, Materialbeschaffung und Gerätebau. Frau Jutta Hass und Frau Dr. Pamela Winchester danke ich für Ihre Geduld und Unterstützung. Von unschätzbarem Wert waren die Unterstützung und Einflüsse meiner Kooperationspartner aus dem BMBF Projekt „FSZ Industrie“. Mein besonderer Dank gilt Dr. Hannah Breitenstürmer, Dr. Klaus Keite-Telgenbüscher, Herrn Wolfgang Beck Dr. Andreas Hinsch und dem gesamten Fh ISE Farbstoffsolarzellen Team.

Unbezahlbar waren die Hilfe, Begleitung und moralische Unterstützung meiner Freunde und Familie. Tausendmal mehr Dank geht an die Neuthe Connexion und SKK. We did it!



<b>1</b>	<b>WORKING WITH DAYLIGHT - INTRODUCTION</b>	<b>1</b>
1.1	RELEVANCE OF DYE-SENSITIZED SOLAR CELLS	1
1.2	GENERAL WORKING PRINCIPLE	4
1.3	DYE DEVELOPMENT	7
1.3.1	CHALLENGE	7
1.3.2	TRENDS	8
1.3.3	ROLE OF THE DYE AND DESIGN PRINCIPLES	14
<b>2</b>	<b>SCIENTIFIC GOALS</b>	<b>16</b>
<b>3</b>	<b>RESULTS AND DISCUSSION</b>	<b>19</b>
3.1	NOVEL SCN-FREE VS. SCN-CONTAINING RUTHENIUM DYES FOR TiO <sub>2</sub> BASED DYE SENSITIZED SOLAR CELLS	19
3.2	PHOSPHONIC ACID ANCHORED RUTHENIUM COMPLEXES FOR ZNO-BASED DYE-SENSITIZED SOLAR CELLS	20
3.3	SIMPLE NIR COMPLEXES AND THEIR APPLICABILITY IN DYE-SENSITIZED SOLAR CELLS	21
<b>4</b>	<b>SUMMARY AND CONCLUSION</b>	<b>22</b>
<b>5</b>	<b>OUTLOOK</b>	<b>24</b>
<b>7</b>	<b>ZUSAMMENFASSUNG</b>	<b>26</b>
<b>6.</b>	<b>REFERENCES</b>	<b>28</b>
<b>7.</b>	<b>APPENDIX</b>	<b>31</b>
A.	FIGURES	31
<b>8.</b>	<b>CURRICULUM VITAE</b>	<b>32</b>







## Abbreviations

1,10 phen	1,10 phenanthroline
bpy	bipyridine
Btu	British thermal unit
CB	conducting band
CE	counter electrode
DMF	<i>N,N</i> -dimethylformamide
DPA	dipyridylamine
DSSC(s)	dye-sensitized solar cell(s)
equiv.	equivalent
HOMO	highest occupied molecular orbital
IPCE	incident photon to current conversion efficiency
$J_{sc}$	short circuit current density
FF	fill factor
LDA	lithium diisopropylamide
LUMO	lowest unoccupied molecular orbital
MLCT	metal-ligand charge transfer
mpabpy	( <i>E</i> )-4-(2-(4'-methyl-[2,2'-bipyridin]-4-yl)vinyl)- <i>N,N</i> -diphenylaniline
$\eta$	efficiency
NIR	near infrared region
N,O	iminosemiquinonate
N,N	diiminosemiquinonate
OPV	organic photovoltaics
PEDOT	poly(3,4-ethylenedioxythiophene)
r.t.	room temperature
SC	semiconductor
SCN	thiocyanate
TCO	transparent conducting oxide (= glass substrate)
$V_{oc}$	open circuit voltage





# 1 Introduction

## 1.1 Relevance of dye-sensitized solar cells

In the year 2010 the world's energy consumption amounted to 524 quadrillion Btu\* (British thermal unit) and is predicted to increase by 56% within the next three decades as shown in Fig. 1.<sup>1</sup> As a result of the extensive use of oil and coal as primary energy resources, the global concentration of CO<sub>2</sub> in the air has increased by 40% since the industrialization started in 1750 and is now rising faster than ever before.<sup>2</sup> Since 1950 the yearly global CO<sub>2</sub> production more than tripled. CO<sub>2</sub> is viewed to be a major cause of global warming, one of the world's biggest environmental issues. The predicted energy crisis<sup>3,4</sup> and a growing awareness for environmental sustainability have brought most of the industrial nations to the understanding that we must transform our energy system.

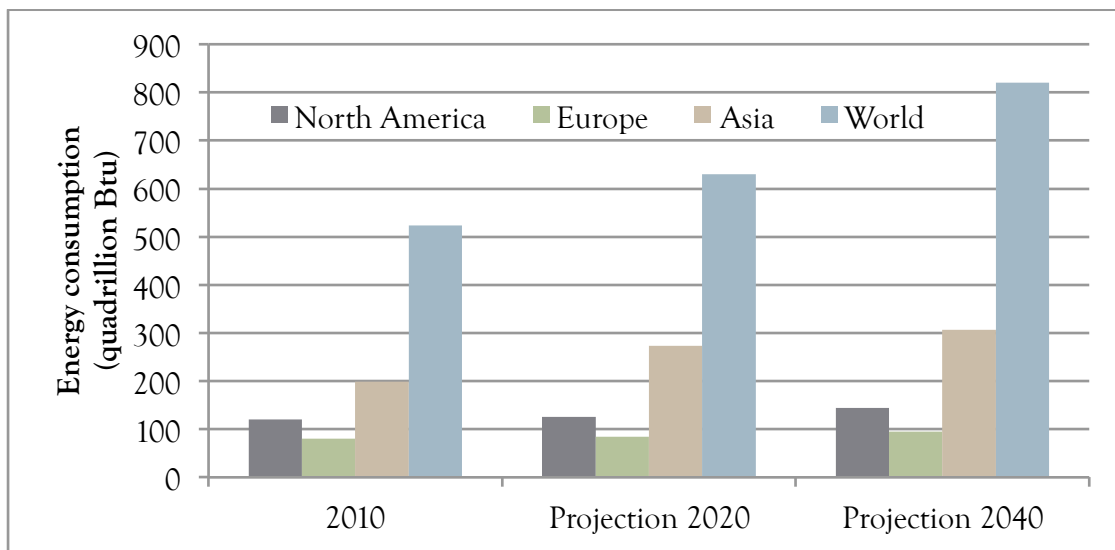


Fig. 1. Development of world energy consumption as predicted by the International Energy Outlook 2013.<sup>1</sup>

Aside from efforts to conserve energy through better insulation of housing, more efficient electric appliances, and various other methods, the use of renewable energy resources is regarded as the major instrument to save resources and reduce CO<sub>2</sub> emission.<sup>5</sup> Besides wind energy, solar energy is viewed to have considerable potential as a future energy resource.<sup>6-8</sup> Solar

---

\*524 quadrillion Btu = 156 PWh. Share in 2010's energy consumption: Asia 38%, North America 22%, Europe 16%.

energy is omnipresent, limitless, and free of charge. Solar power plants work emission free and without noise or dust nuisance. Another advantage is that solar power can be produced during peak load times, which are usually during the day. However, critics say it is not capable of providing base load power and leads to destabilization of the power grid due to its erratic output. It is nevertheless already widely used.<sup>6,8</sup> In Germany, solar energies contributed 5.3% to the total net electric power consumption of 560 TWh in 2013.<sup>9</sup>

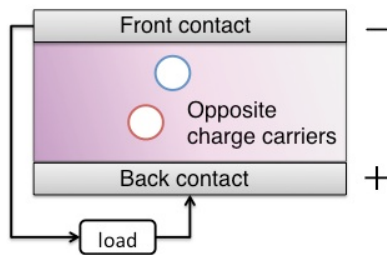


Fig. 2. Schematic view of basic operation principle of a photovoltaic device.

Table 1. Examples of research-cell efficiencies

Technology	Efficiency
Mono-crystalline silicon	25.0%
Poly-crystalline silicon	20.4%
CdTe	19.6%
CIGS	20.8%
Amorphous silicon	13.4%
GaAs	29.1%
Multijunction cells	31.1-44.4%

Solar cells operate on the basic principle schematically shown in Fig. 2. Upon absorption of light, charge carriers are generated and subsequently separated within the photovoltaic material. Extraction of the separated charge carriers to an external circuit then produces electricity.

There are a number of different solar cell types and materials. A detailed overview of the different cell types and the highest efficiencies achieved on laboratory scale can be seen in figure A. 1 in the appendix. Examples of the latest research-cell efficiencies are given in Table 1.

The best-known cell types are probably crystalline silicon cells. Devices of this type reach a maximum efficiency of 25% on a laboratory scale. Mono- and poly-crystalline solar cell modules are standard cells used in power plants, in private households, or consumer devices. In order to reduce the amount of material required for cell production and thereby lower production costs, thin-film technologies were developed. Thin-film cells like cadmium telluride (CdTe), copper indium gallium selenide (CIGS), and amorphous silicon (a-Si) yield efficiencies of up to 20%. Having lower efficiencies than their crystalline counterparts, thin-film cells could not live up to the expectations. The comparable highest efficiencies have been achieved with gallium arsenide (GaAs, 29.1%) and multijunction cells (31.1-44.4%). Despite their high efficiencies those devices have two major drawbacks: They are made of highly toxic materials and have a very limited availability.

In summary, semiconductor-based solar cells are highly efficient and are already being used in industry. However, they are not environmental friendly. The production of high efficiency cells is costly, energy consuming, and requires clean-room technologies, while cells that are produced with simple processes are considerably less efficient. Another shortcoming is that toxic semiconductor materials have to be used.

Organic photovoltaics (OPV) using metal-containing and metal-free organic dyes have emerged as an alternative technology. The so-called dye-sensitized solar cells (DSSCs) are of interest because they are relatively cheap to produce and open a new field of applications. No special technologies are needed and the materials are widely available. DSSCs can be produced on flexible materials, thus potentially enabling large-scale industrial roll-to-roll production processes. Their efficiencies depend less on the angle, and intensity of the incident light and they can be produced on rigid and flexible materials and in various colors. This means, instead of putting the panels on top of buildings in a certain angle they can be vertically integrated into buildings as windows, for example. The efficiencies of DSSCs are little affected by cloudy conditions or less intensive light irradiation in the evening hours. Flexible cells can be integrated in consumer goods as clothing or bags to charge and power electronic devices. Organic photovoltaics are able to open up a variety of novel fields and applications and shall play an important part in the production of energy in the 21<sup>st</sup> century.

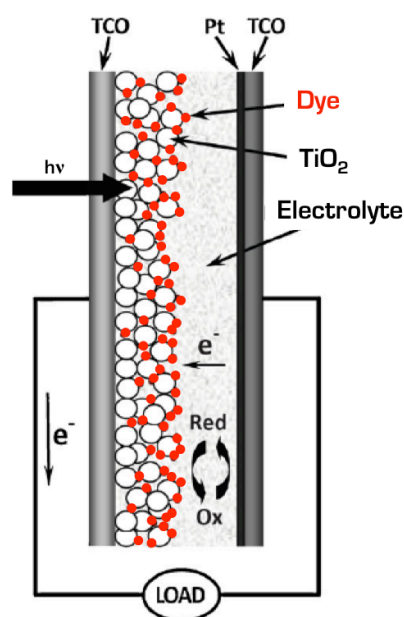
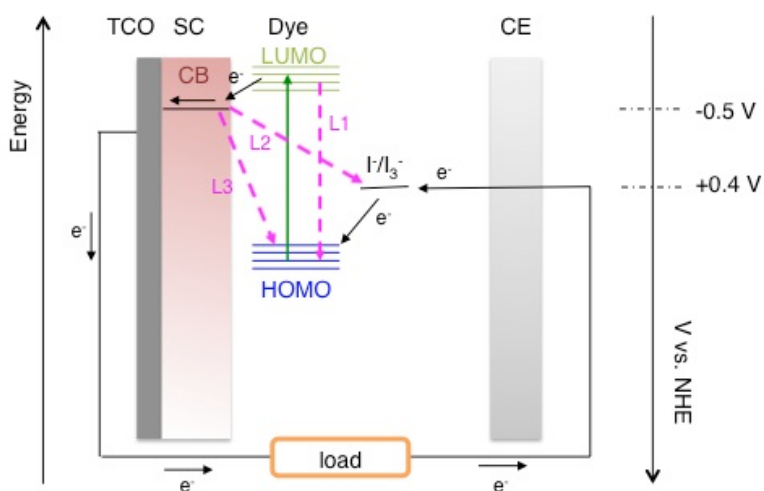


Fig. 3. Schematic representation of the working principle of a DSSC. {Hagfeldt:2010df} TCO = transparent conductive oxide, CE = counter electrode, Pt = platinum.

## 1.2 General working principle

The principle setup of a DSSC device is shown in **Fig. 3**.<sup>10</sup> It consists of a transparent photoanode, a dye that is adsorbed onto the photoanode, a counter electrode (CE), and an electrolyte in between the electrodes. The photoanode is made of a nanoscopic mesoporous semiconductor, e.g.  $\text{TiO}_2$ ,  $\text{ZnO}$ , or  $\text{SnO}$  that is deposited on a transparent conductive glass substrate (TCO). The dye is adsorbed via suitable anchoring groups to the semiconductor material. The counter electrode is made of a transparent conductive glass (TCO). In order to overcome the inherent high charge resistance of TCO substrates, a catalytic layer of a highly conductive material like platinum (Pt), carbon materials (e.g. carbon black), conducting polymers (e.g. PEDOT), or cobalt sulfide is deposited onto them. The cell is filled with an electrolyte containing a redox mediator, mostly the  $\text{I}^-/\text{I}_3^-$  redox couple.



**Fig. 4.** Basic reactions in a DSSC (the loss reactions L1-L3 are drawn with dashed pink arrows).

The basic processes<sup>10-12</sup> that take place in a DSSC are illustrated in **Fig. 4**. Excitation of the dye by absorption of light leads to the elevation of an electron to the lowest unoccupied molecule orbital (LUMO) of the dye. From there, charge separation of the photo-excited electron occurs by the injection from the excited dye into the conduction band (CB) of the semiconductor (SC) at an ultrafast rate leaving oxidized dye molecules. Electron injection will only take place if the energy level of the LUMO is above the Fermi level of the SC, i.e., of higher energy than the CB. Upon injection the electrons diffuse through the interconnected nanocrystals of the mesoporous semiconductor film to the photoanode and the redox mediator in the electrolyte regenerates the oxidized dye molecules to their ground state. Iodide, which is standardly used as electron donator, is thereby oxidized to triiodide. The regenerative redox reaction is only



possible if the energy level of the highest occupied molecular orbital (HOMO) of the dye is lower than the redox potential of the redox mediator. When the  $I^-/I_3^-$  redox couple is used, the HOMO of the dye should be at potentials more positive than +0.4 V vs. NHE.

Once the electrons diffuse through the semiconductor and reach the conducting TCO material, a photocurrent will be detected in the external circuit. The electrons travel through the external load to the counter electrode where they enter the internal circuit again and regenerate the oxidized redox mediator (e.g. reduce triiodide to iodide).

There are three loss reactions that decrease the efficiency of a DSSC. They are marked as L1-L3 in **Fig. 4**. The first (L1) is the direct decay of an excited molecule to the ground state before injection of an electron into the SC takes place. The second loss reaction (L2) is a reduction, where an excited dye molecule reacts with an oxidant species in the electrolyte. The third possibility is the loss of an electron from the semiconductor surface and its recombination with an oxidized dye (L3). As all loss reactions decrease the total current generation, the unwanted processes have to be kept as low as possible by chemical and technical engineering.

The performance of a solar cell is most commonly characterized by three parameters:

1. the overall solar energy-to-electrical energy conversion efficiency ( $\eta$ , 'efficiency') under sunlight illumination,
2. the fill factor (FF), and
3. the wavelength-dependent incident photon to current conversion efficiency (IPCE).

The parameters can be calculated from the short circuit current density  $J_{SC}$  and the open circuit potential  $V_{OC}$  of the device, which are measured under sunlight illumination. A sample J/V curve, from which  $J_{SC}$  and  $V_{OC}$  are deduced, is given in **Fig. 5**.

The short circuit current density is the maximum current output of the cell and measured at the point where the net voltage is zero. Its height is determined by the efficiency of the electron injection into the conducting band of the semiconductor and the collection efficiency at the photoanode. Similarly, the open circuit potential is the maximum voltage available from the cell measured at the point where the net current is zero. It is defined by the potential difference between the Fermi level in the semiconductor and the redox potential of the redox mediator. The product of  $J_{SC}$  and  $V_{OC}$  defines the theoretically possible maximum power  $P_{calc}$  of a cell. The

actual maximum power  $P_{max}$  of the cell is the product of photovoltage  $V_{MP}$  and photocurrent  $J_{MP}$  at the voltage where the power output is maximal as shown in **Fig. 5**.

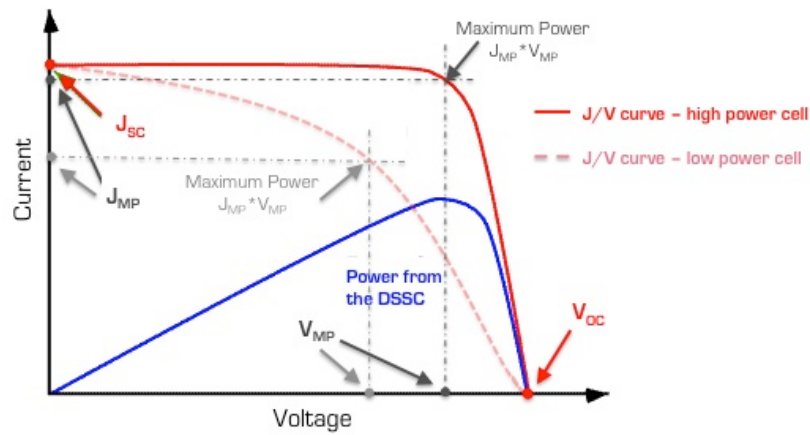


**Fig. 5** J/V curve of a DSSC showing the positions of the short circuit current density  $J_{sc}$ , the open circuit potential  $V_{oc}$ , and the maximum power for a high power and a low power device.

The efficiency of a solar cell is determined from  $J_{sc}$  and  $V_{oc}$  according to Equation 1.

$$\eta = \frac{J_{sc} \cdot V_{oc} \cdot FF}{P_{in}} = \frac{P_{max}}{P_{in}} \quad \text{Eq. 1}$$

$P_{in}$  is the intensity of the incoming light. FF can adopt values between 0 and 1 and is defined by the ratio between the maximum power ( $P_{max}$ ) of the cell and the product of  $J_{sc} \cdot V_{oc}$  as expressed by Equation 2. Graphically, FF can be described as the largest possible rectangle that can be fitted under the J/V curve (see **Fig. 6**)

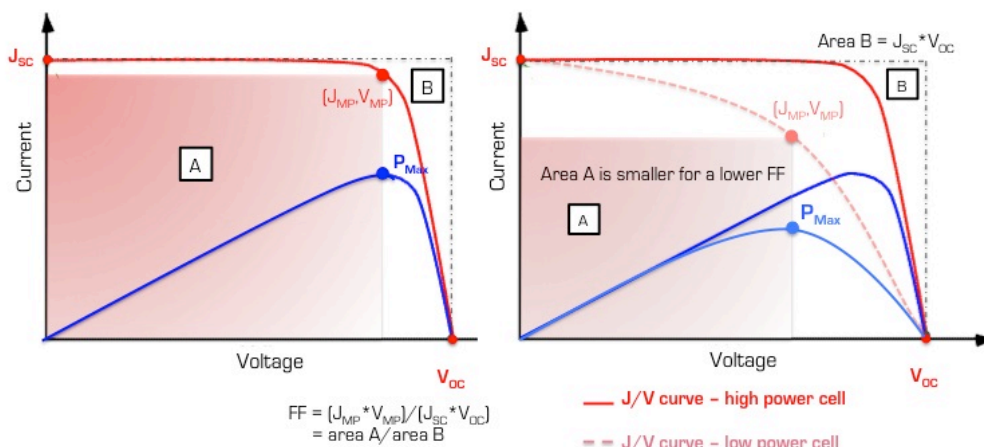


**Fig. 6.** J/V curves of DSSCs with high power output (left graph) and low power output (dashed line in graph on the right), respectively. Illustration of the determination of the FF as the largest possible rectangle that fits below the J/V curve of a photovoltaic device.

$$FF = \frac{J_{MP} \cdot V_{MP}}{J_{SC} \cdot V_{OC}} = \frac{P_{max}}{P_{calc}} \quad \text{Eq. 2}$$

The fill factor FF is an important parameter for the evaluation of a solar cell as it describes cells with the same  $J_{SC}$  and  $V_{OC}$  but with different power production. Efficient solar cells have fill factors higher than 0.7. Low fill factors can be attributed to losses due to high resistance and recombination.

The third measure, the IPCE, expresses the external quantum efficiency. This is the external photocurrent density measured in the external circuit of the cell under monochromatic illumination at different wavelengths divided by the incoming photon flux ( $\phi$ ). The IPCE can be calculated as described in Equation 3.

$$IPCE(\lambda) = \frac{J_{sc}(\lambda)}{e\phi(\lambda)} = \frac{J_{sc}(\lambda)[Acm^{-2}]}{\lambda[nm]P_{in}(\lambda)[Wcm^{-2}]} \quad \text{Eq. 3}$$

with  $e$  as the elementary charge.

## 1.3 Dye development

### 1.3.1 Challenge

DSSC devices employ a dye that generates electric power when excited by sunlight. Clearly, dyes play an important role for the performance of DSSCs.

In 1991 first high-performance ruthenium dye was published by Grätzel and co-workers.<sup>13</sup> The structure of the reported ruthenium(II)polypyridil complex named **N3** shown in **Fig. 7**. The complex yielded 10% efficiency when applied in a DSSC device on laboratory scale.

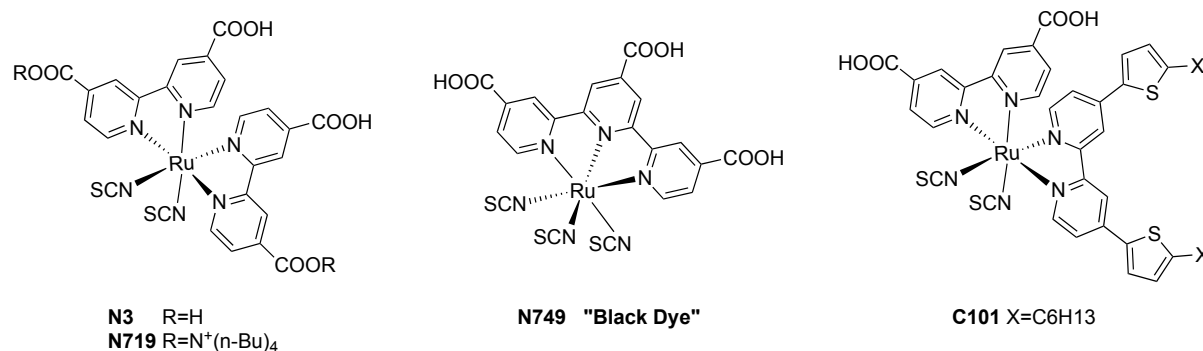


**Fig. 7.** Structure of ruthenium dyes used as gold standards.<sup>14-16</sup>

The complex resembles the structural features of typical metal complexes used in DSSCs:

- the bipyridine moiety with carboxylic acid groups that serves as an **anchoring group** and
- the bipyridine moiety with the electron rich thiocyanate (SCN) ligand that serves as **light harvesting donor unit**.

Despite intensive research, no dye has been published yet that significantly exceeds the 10% efficiency threshold on laboratory scale. The most efficient dyes reach values of around 10-12%. The benchmark dyes are **N719** ( $\eta = 11.2\%$ ) and **N749** (often referred to as “black dye”) ( $\eta = 10.4\%$ ) as well as **C101** ( $\eta = 11.4\%$ ).<sup>14-16</sup>

Because scaling up of the DSSC devices from laboratory to commercially competitive scale will surely include high losses in performance, the current efficiency values of the DSSCs have yet to be improved.

The main challenges here are the relatively narrow window of the absorption spectrum of the dye ( $\Delta\lambda \approx 350$  nm, see **Fig. 8**)<sup>17</sup> as well as its stability and electrochemical features like energy levels, internal charge separation, and regenerability after electron injection into the semiconductor.

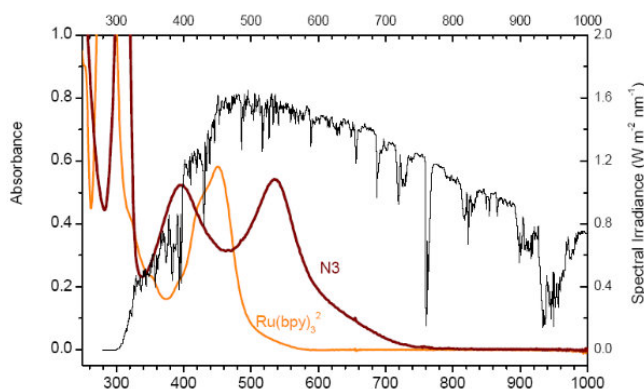


**Fig. 8.** Comparison of the absorption spectra of ruthenium(II)trisbipyridine dichloride (orange line) and N3 dye (red line) and the solar spectrum.

### 1.3.2 Trends

Since the discovery of the first powerful dyes, i.e., **N3**, **N719**, and “black dye” **N749**, many groups have worked on inventing new dyes that improve the performance of a DSSC. The development of new ruthenium-based dyes is thus strongly geared to these benchmark dyes. There are two main strategies. The first being is to substitute one of the anchoring ligands with an electron rich donor ligand. Another approach is to exchange the SCN moieties with another

donor moiety. The goal of both strategies is to extend the absorption spectra of the dyes using different electron rich, extended aromatic or  $\pi$ -conjugated substituents as donors.

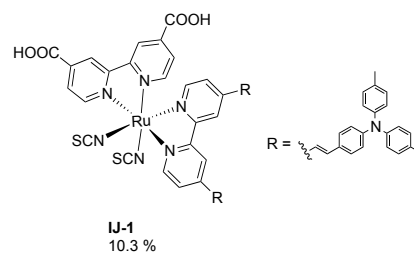
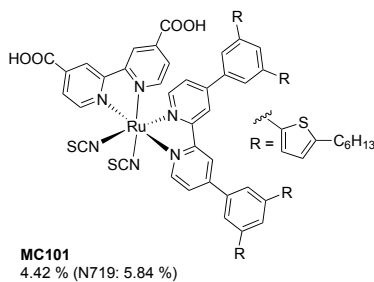
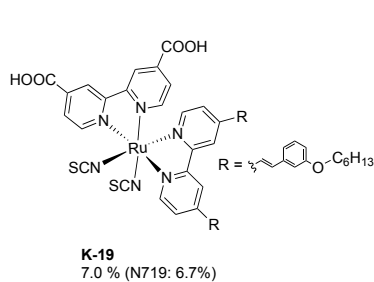
As DSSCs are formed by a combination of materials, the performance of the cell is affected by multiple influences, for example, cell size, composition of the electrolyte, and the manufacturing method of the cell. Therefore, their efficiencies which are measured with different cells using the same dye, usually vary a lot. The aforementioned benchmark dyes are generally used as references and in the following overview available reference efficiency values will be stated for comparison.

### SCN-containing dyes

An example for the implementation of the first strategy is the high efficiency dye **C101** (Fig. 7). Here, two of the carboxylic anchors of the bipyridine ligand are substituted with electron rich thiophene donor ligands. In addition to that, alkyl chains were added to make the complex more hydrophobic and shield the underlying  $\text{TiO}_2$  layer against water from the electrolyte. This set-up prevents dye leaching from the SC surface and reduces recombination reactions with the redox mediator by enhancing charge separation.<sup>18-20</sup> Other dyes, like **K-19**<sup>21</sup> and **MC101**<sup>22</sup>, both shown in Fig. 10, follow the same approach. The introduction of the phenylgroup in **K-19** and **MC101** led to a red shift of the MLTC absorption with a higher extinction coefficient. The electron-donating alkoxy group in **K-19** suppressed recombination losses, the alkoxy chains increased the thermal stability of the dye.<sup>21,23</sup> Therefore, the dye **K-19** slightly outperformed **N719** (**K-19**:  $\eta = 7.0\%$ , **N719**:  $\eta = 6.7\%$ ). **MC101** also showed excellent absorption properties, a high extinction coefficient, and increased thermal stability. However, due to lower LUMO values its  $V_{OC}$  was decreased, resulting in lower efficiencies than the reference dye (**MC101**:  $\eta = 4.42\%$ , **N719**:  $\eta = 5.84\%$ ). The dye **IJ-1**<sup>24</sup> (Fig. 10) is an example for “donor-acceptor” type of dyes. Their set-up is inspired by metal-free organic dyes, in which the donor and the acceptor moiety is connected via a  $\pi$ -conjugated bridge. The triphenylamine group functions as donor and the double bond acts as  $\pi$ -bridge to the ruthenium core, which serves as the acceptor. The dye also displayed good absorption properties with high extinction coefficients as well as decreased recombination tendencies compared to **N719**, which is reflected by its high efficiency ( $\eta = 10.3\%$ ).<sup>24</sup>

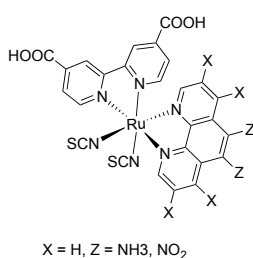
## SCN containing dyes

## a) bpy donor ligand

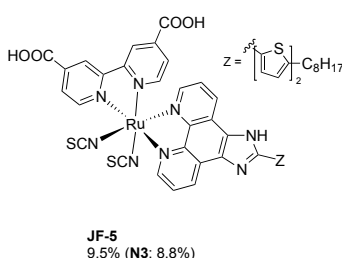


## b) 1,10-phenanthroline donor ligand

## type A



## type B



## c) dipyriddyamine donor ligand

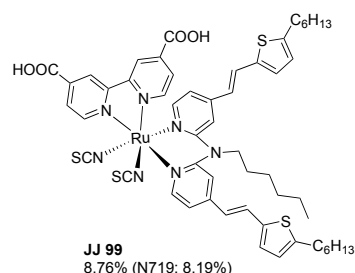


**Fig. 9.** Structures of recently published alternatives to the ruthenium standard dyes that contain SCN.<sup>22,24,25</sup> The given values refer to the efficiency  $\eta$  of the cell.

Besides simply exchanging the carboxylic acids of the bipyridine anchor ligand, researchers have substituted the whole bipyridine ligand with 1,10-phenanthroline-based and dipyriddyamine-based donor ligands.<sup>23</sup> However, the electron rich substituents that lead to successful donor ligands remain the same, and they include highly conjugated thiophene and triphenylamine systems that are optionally equipped with alkylchains.

Interestingly, 1,10-phen derivatives of the general structure type A shown in **Fig. 9** had very low efficiencies ranging from  $\eta = 6.7\text{-}0.1\%$  (N719:  $\eta = 8.8\text{-}3.6\%$ ). This was due to high recombination rates and weak MLTC transitions. Carbazole-functionalized phenanthrenyl-based donor ligands denoted type B in **Fig. 9** have shown better cell performance. The carbazole unit raised the charge-separation time scale, hence reducing recombination losses. These types of complexes also led to high  $V_{OC}$  values. In combination with an intense MLTC and optimized adsorption behavior the dye **JF-5**<sup>26</sup> (**Fig. 9**) showed better power conversion efficiency than **N3** (**JF-5**:  $\eta = 9.5\%$ , **N3**:  $\eta = 8.8\%$ ). **JJ99**, a dipyriddyamine-based complex, also employs alkyl-thiophene substituents for successful light harvesting. Due to its broadened absorption spectra in the near infrared region, it slightly outperformed **N719** (**JJ99**:  $\eta = 8.76\%$ , **N719**:  $\eta = 8.19\%$ ).<sup>25</sup>

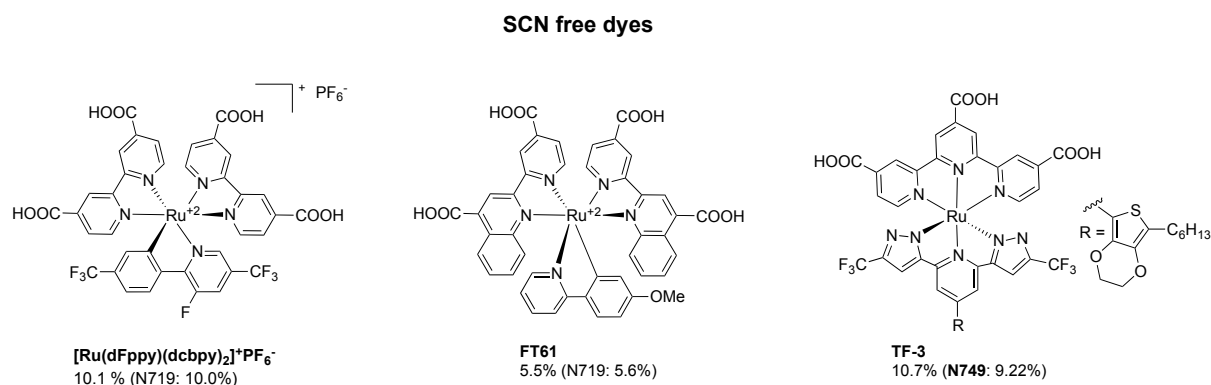


Fig. 10. Standard dyes and recently published alternatives without SCN.<sup>27-29</sup>

### SCN-free dyes

The second approach is to exchange the SCN moieties. It is based on the finding that these are the weakest part of the structure as they are easily substituted by components of the electrolyte in the cell, which decreases the overall performance.<sup>30</sup> This approach is partially delicate because the SCN ligands are unique donors that cause strong charge transfers from the ligand to the metal center (MLCT) at a high wavelength ( $\lambda = 550$  nm).

Alternative complexes featuring donor ligands, e.g., substituted cyclometalates or trileptic ligands, are shown in Fig. 10. Despite their excellent optical features even in the near infrared region (NIR) of the solar spectrum, the majority of these complexes have not been able to exceed the performance of the benchmark dyes. An exception are fluorine substituted complexes, like [Ru(dFppy)(dcbpy)<sub>2</sub>]+PF<sub>6</sub><sup>-</sup> ( $\eta = 10.1$  %, N719:  $\eta = 10.0$ %), where the fluorine moiety seems to allow more efficient electron injection and dye regeneration,<sup>23,29</sup> thus leading to higher efficiencies. The fluorine moiety stabilizes the Ru(III) oxidation state because it decreases the electron-donating character of the cyclometalate ligand as well as its Lewis basicity., which facilitates dye regeneration and efficient electron injection.<sup>29</sup> Introducing a methoxy substituent into the cyclometalated ligand as in FT61 (Fig. 10) has also been beneficial ( $\eta = 5.5$  %, N719:  $\eta = 5.6$ %).<sup>28</sup> The dye FT61 showed high panchromatic sensitization with high IPCE values up to 900 nm (IPCE at 800 nm = 55%, IPCE at 900 nm = 25%), whereas the reference N719 showed a sharp drop of IPCE values after 700 nm (IPCE at 800 nm = 5%, IPCE at 900 nm = 0%). Another thiocyanate-free dye with panchromatic sensitization characteristics was TF-3. The bis-tridentate complex showed higher stability and  $J_{SC}$  values as well as lower charge recombination rates than the ‘black dye’ N749, hence outperforming it ( $\eta = 10.7$  %, N749:  $\eta = 9.22$ %).<sup>27</sup>

### Modified anchor ligands

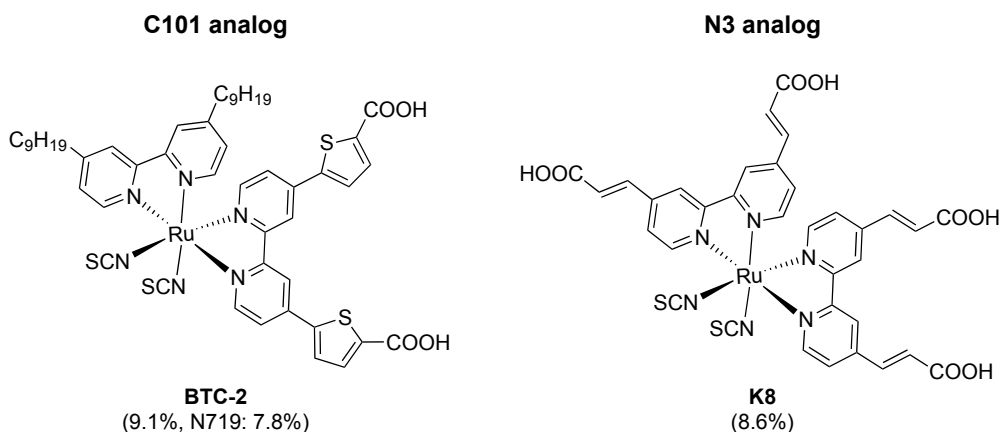


**Fig. 11.** Structures of new ruthenium-based complexes with modified anchor ligands. The numbers refer to the efficiency  $\eta$ .<sup>31-33</sup>

In addition to these two main approaches another strategy is also pursued where the anchoring ligands are modified. Motives that are often employed are the insertion of thiophene between the carboxylic anchor and the bipyridine ligand or the use of phenanthroline derivatives instead of bipyridines as anchoring ligands. These types of anchoring ligands did often show decreased electron injection properties or weak adsorption, which resulted in low efficiencies.<sup>23,31</sup> Two more successful examples are complexes **K8** and **BTC-2** as shown in **Fig. 11**.<sup>32,33</sup> As both are closely related to the gold standards **N3** and **C101**, their good performance underlines the benefit of introducing alkyl chains,  $\pi$ -bridges, and thiophene moieties into the complex.

### Dyes with other metals

Besides ruthenium-centered metal dyes other metal complexes have been investigated with respect to their applicability as sensitizers in DSSCs, in particular metals comprising osmium,<sup>34</sup> copper,<sup>35</sup> nickel,<sup>36</sup> and platinum.<sup>37,40</sup> Nickel as well as platinum complexes have attracted special interest, as they are potentially able to harvest sunlight far into the NIR.<sup>41</sup> The first to succeed in implementing platinum complexes in a DSSC device were Saguhira and co-workers in 2001.<sup>37</sup> Here, the diimino-dithiolate complex **Pt(dcbpy)(qdt)** (**Fig. 12**) was the most efficient sensitizer ( $J_{SC} = 7.0 \text{ mA/cm}^2$ ,  $V_{OC} = 0.6 \text{ V}$ ,  $FF = 0.77$ ,  $\eta = 3.0 \%$ , no reference values given). Similar complexes were prepared by Robertson and co-workers.<sup>38,39</sup> Due to aggregation of the dyes and high recombination rates, however, the efficiencies remained well below the threshold of the ruthenium-centered standard dyes. Additionally, the complex had only weak absorption in the NIR.



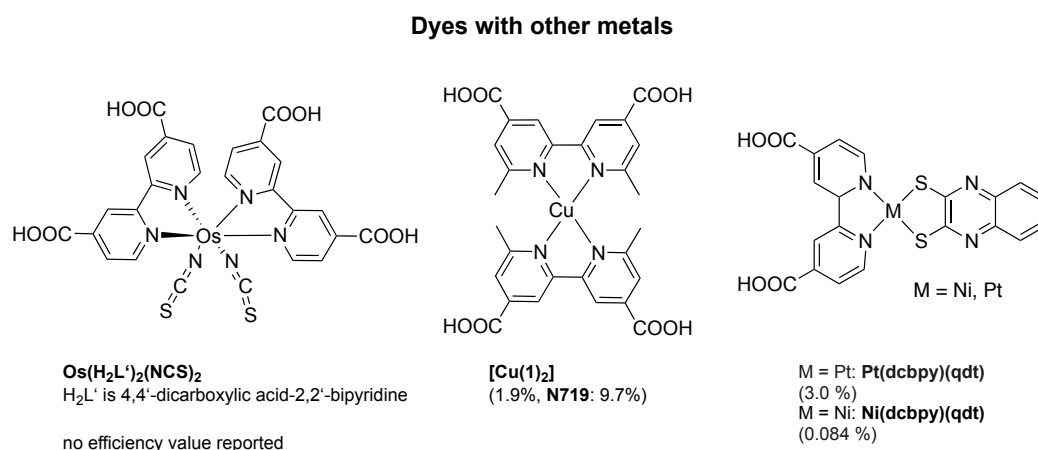


Fig. 12. Examples for alternative metal complexes and metal free organic dyes applicable in DSSC devices.<sup>34-37</sup>

Besides platinum complexes Robertson and co-workers also prepared the heteroleptic nickel complex **Ni(dcbpy)(qdt)** as shown in Fig. 12.<sup>36</sup> The dyes had appropriate redox potentials and sufficient charge-separated lifetime, but low extinction coefficients and no NIR absorption. A working solar cell device could be built using that sensitizer. Disappointingly, since the obtained photocurrent was low and the efficiency did not exceed 0.084% because of low injection rates. The same results were observed using complex **Pt(dcbpy)(qdt)**. The results for both asymmetric nickel and platinum diimino-thiolates suggested that the efficiency could be improved by extending the spectral absorption range and adjusting of the electrochemical properties by using alternative types of ligands.

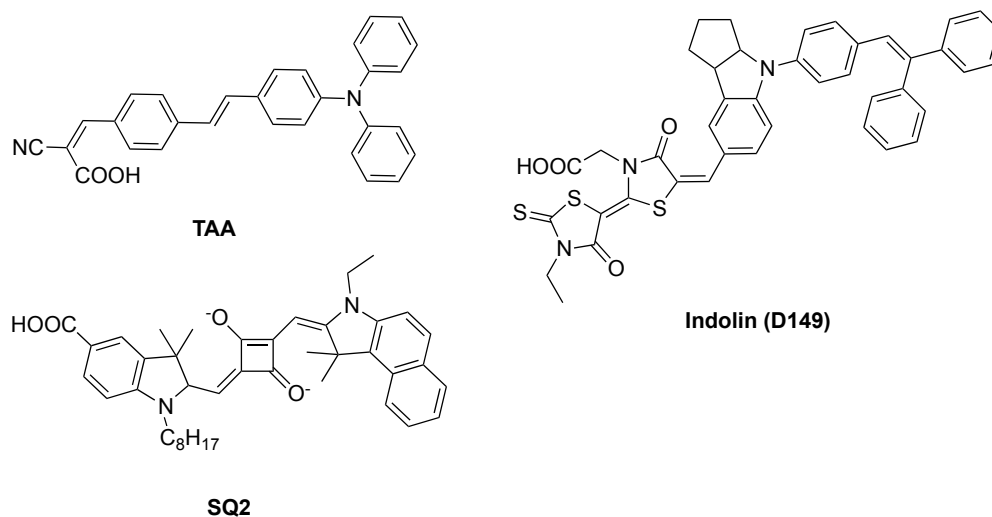


Fig. 13. Organic dyes TAA = triarylamine,<sup>12</sup> indoline (D149),<sup>42</sup> and SQ2 = squaraine.<sup>43</sup>

### Metal-free dyes

Due to their often excellent light harvesting properties, metal free organic dyes are very interesting as sensitizers in DSSCs.<sup>44</sup> Some successful examples comprise: triarylaminines, indolines, and squaraines. They stand out for their high extinction coefficients and broad absorption spectra. The best cells sensitized with metal free dyes reached efficiency values between 7-9%. Drawbacks remain, because the performance is still impaired by low IPCE,  $V_{OC}$ , and  $J_{SC}$  values. In addition, they are sensitive to oxidation and thus suffer from stability issues.<sup>44</sup> Examples for successful metal free dyes are given in **Fig. 13**.

### 1.3.3 Role of the dye and design principles

Based on the known complexes, some structure-function relationships with respect to the performance of ruthenium type sensitizers may be concluded. The most relevant properties of the dye affecting the cell performance are:

- **Tight and quantitative adsorption** onto the semiconductor surface,
- Quick and effective **electron injection** into the semiconductor, and
- **Strong absorption** over a wide wavelength range.

While anchor ligands influence the adsorption and the electron injection properties of the dye, donor ligands affect its absorption behavior.

The dyes are adsorbed onto the semiconductor surface via appropriate anchoring groups. While carboxylic acid is most commonly used as anchor other groups like phosphonates, sulfates, and nitrates are also possible. It is assumed, that phosphonates are especially suitable for the acid labile ZnO surface. The amount of anchoring groups in a dye affects the adsorption behavior of the dye as well as the photo voltage of the cell. Complexes with four anchoring groups are favorable, first of all because they enable strong adsorption and second because experiments have shown that this leads to an increase of the photovoltage in comparison to complexes with only two anchoring groups.<sup>12</sup>

In addition, the nature of the anchoring groups influences the height of the photocurrent and voltage as well as the electron injection. The higher the level of protonation, the higher the photocurrent, the quicker the injection but also the lower the photo voltage. In pH-dependent experiments where the effect of the deprotonation of **N3** on the performance was tested, the doubly protonated, i.e., doubly deprotonated complex **N719** performed better. Hence, heteroleptic complexes with four partly deprotonated anchoring groups have the best balance of features and requirements. The counterions that stabilize the deprotonated anchoring group

should be as big as possible to prevent its diffusion to the semiconductor surface, which would make the surface more positive and thus decrease the photovoltage. The counterion most commonly used is tetrabutylammonium.

In order to ensure a strong and broad absorption, electron-rich, extended  $\pi$ -systems are often used. As described in Chapter 1.3.2, no general guidelines can be formulated here. A wide variety of donor ligands has been published. The most successful ligands range from the approved thiocyanate to thiophene or phenyl substituted bipyridines and cyclometalates.

## 2 Scientific Goals

The goal of this work was to design, synthesize, and characterize new dyes for the application as sensitizer in dye-sensitized solar cells. The aim was to find dyes that lead to an increase of cell efficiency. The approach and envisioned target molecules are described in the following.

The approach for improvement of the overall cell performance was to target the absorption properties of the dye. The goal was to develop dyes with high extinction coefficients and absorption maxima at long wavelengths of the solar spectrum, in particular, to develop ligands for ruthenium complexes and on the synthesize transition metal complexes.

### Ruthenium dyes

Donor ligands

The strategy for the ligand design of the ruthenium complexes is based on the principles presented in Chapter 1.3.3. In order to increase the stability and enhance the adsorption properties of the dye, SCN free complexes carrying two anchor ligands and one donor ligand as sketched in **Fig. 14** will be favored. With this design a strong attachment to the semiconductor should be ensured.

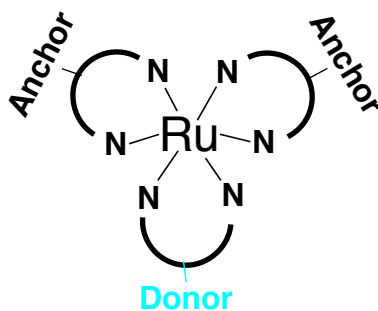


**Fig. 14.** Scheme of basic ruthenium complex.

The SCN donor ligand was to be substituted with a bipyridine (bpy) that is equipped with extended  $\pi$ -conjugated substituents. The target structures are displayed in **Fig. 15**. It is assumed, that the substitution of the SCN groups would enhance the long-term stability of the dye. In order to gain the desired light harvesting properties, the bipyridine donor ligand was to be functionalized with electron-rich extended  $\pi$  systems. Therefore, the use of triphenylamine and indoline derivatives was to be investigated. These moieties are known as building blocks in metal free dyes with high extinction coefficients between  $45 \cdot 10^3 \text{ M}^{-1} \text{ cm}^{-1}$  and  $70 \cdot 10^3 \text{ M}^{-1} \text{ cm}^{-1}$ . Having

low HOMO levels they are excellent donor groups<sup>45</sup> and have been successfully implemented in metal free DSSC devices with efficiencies up to 9.5%.<sup>12,42,46</sup> Besides the aromatic system, one of the ligands was to be substituted with a hydrophobic alkyl chain, that, when attached to the semiconductor should protect the surface from water.<sup>20,23</sup> Additionally, the alkyl chains should prevent  $\pi$ -stacking of the molecules. The  $\pi$ -stacking can lead to aggregation of the molecules, which in turn lowers the efficiency of the dye.<sup>12,47,48</sup>

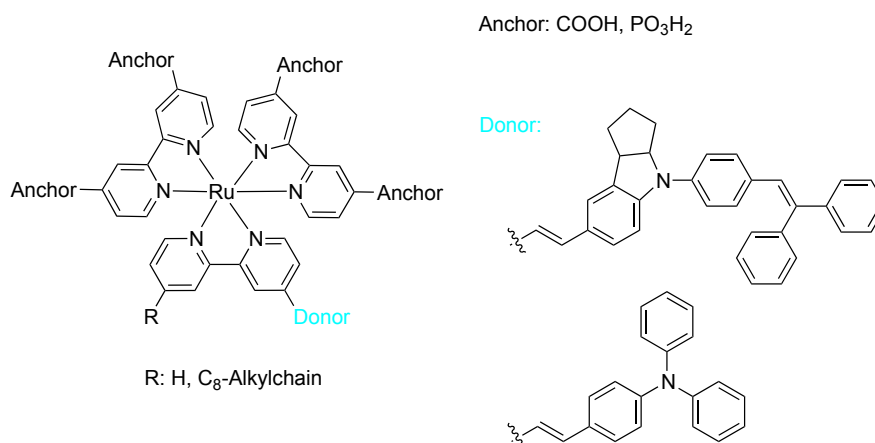


Fig. 15. Structures of the target ruthenium dyes.

#### Anchor ligands

Two different anchoring groups were to be examined to optimize the anchoring properties on different semiconductor materials. Carboxylic anchored dyes were to be prepared for application in TiO<sub>2</sub> based DSSCs. Their phosphonate-anchored analogs were envisaged for the application in ZnO based devices. Two of the four anchoring groups were to be deprotonated to maintain a neutral complex, so that the dye should have an optimal balance between the possible photo voltage and current as described in Chapter 1.3.3.

## Group 10 metal dyes

Transition metal complexes with nickel and platinum metal centers will be synthesized because these types of complexes are known to have high extinction coefficients and, depending on the choice of ligands, absorption in the near infrared region (NIR).

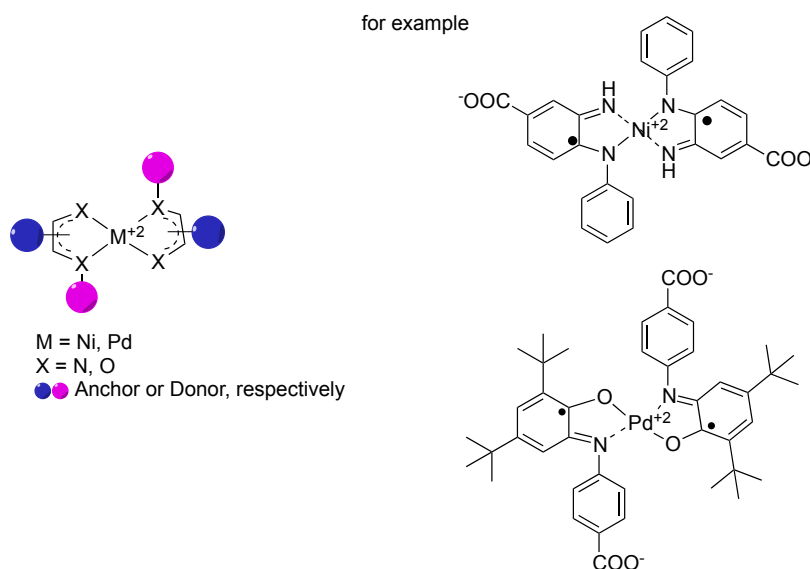


**Fig. 16.** Basic structures of the targeted NIR transition metal complexes as well as two sample structures.

The projected NIR active complexes were to have nickel or palladium metal centers. While both nickel- and palladium are known to form nickel stable (di)imine complexes, nickel has the advantage of it being cheap and readily available.<sup>49-51</sup>

The choice of ligands is of major importance, because they significantly affect the electronic properties of the complex. The challenge will be to make complexes that meet the energetic requirements of a DSSC, i.e. have the correct HOMO and LUMO levels.

As displayed in **Fig. 16**, diimino-semichinonates (X = N) and imino-semichinonates (X = N,O) were chosen as possible ligands. Those ligands were to be equipped with suitable anchor ligands and, in order to adjust the electronic properties, different electron-withdrawing and -donating substituents.

The dyes were to be synthesized following modified literature procedures and analyzed using standard optical and electrochemical methods. Within the electrochemical characterization a pretest to evaluate the applicability of the dyes in DSSCs before measurements in real cells is to be established.

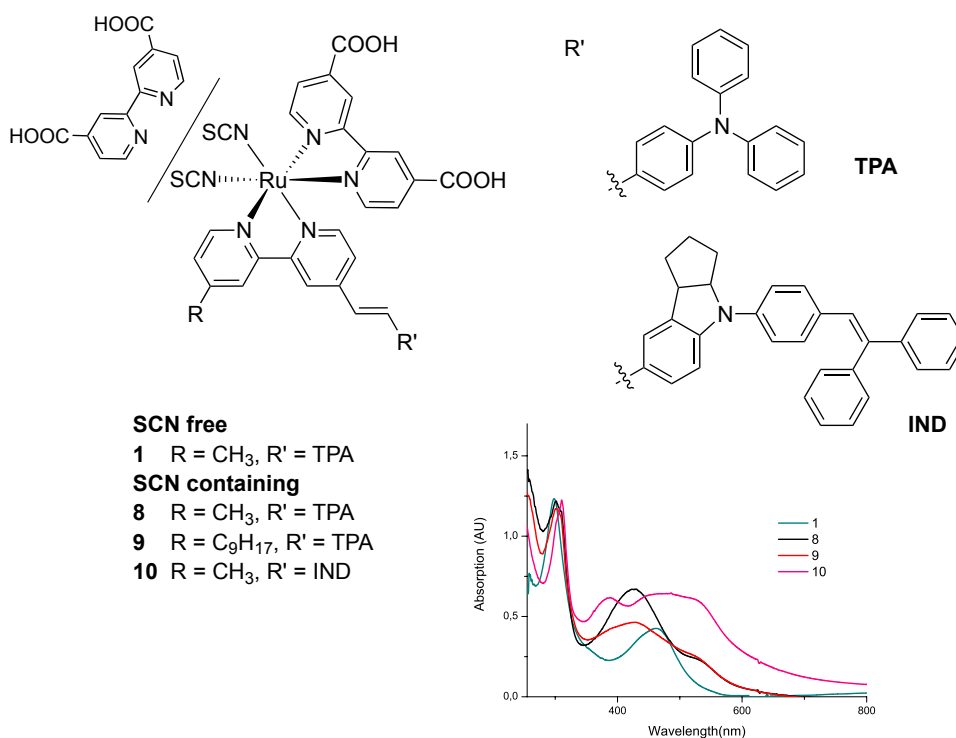
### 3 Results and Discussion

#### 3.1 SCN free vs. SCN containing ruthenium dyes for TiO<sub>2</sub> based dye sensitized solar cells

This chapter was published in:

K. Neuthe, H. Brandt, A. Hinsch, C. Tzschucke, W. Veurman, B. Ziem, R. Haag\*,  
*ChemElectroChem* **2014**, 1, 1656-1661

<http://dx.doi.org/10.1002/celec.201402078>



Author contributions:

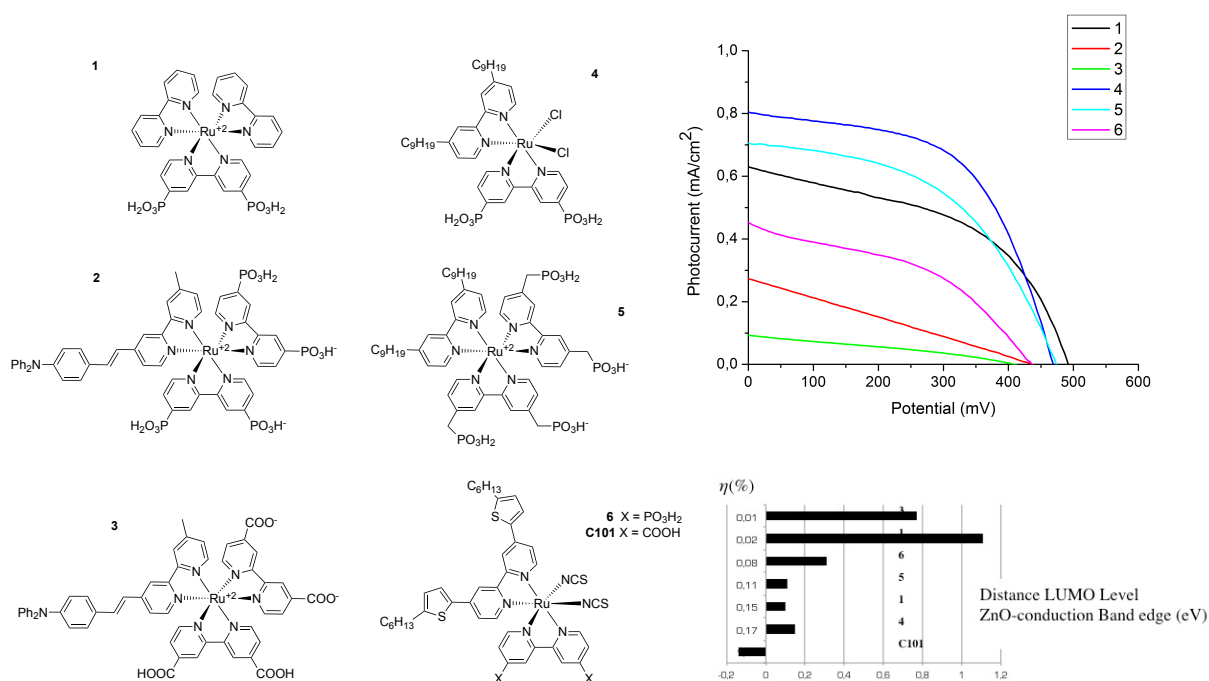
- Complex design
- Synthesis of ligand TPA
- Synthesis of all complexes
- UV/Vis and fluorescence measurements in solution
- Cyclic voltammetry measurements of all complexes
- HOMO/LUMO determination
- Development of a simple model for pre-evaluation of dyes regarding their applicability
- Preparation of the manuscript

## 3.2 Phosphonic acid anchored ruthenium complexes for ZnO-based Dye-Sensitized Solar Cells

This chapter was published in:

K. Neuthe\*, F. Bittner, F. Stiemke, B. Ziem, J. Du, M. Zellner, M. Wark, T. Schubert, R. Haag.  
*Dyes and Pigments* 2014, 104, 24–33.

<http://dx.doi.org/10.1016/j.dyepig.2013.12.018>



Author contributions:

- Complex design with phosphonate anchors
- Synthesis of complex 3 and its ligand
- UV/Vis and fluorescence measurements in solution and on ZnO surfaces
- Cyclic voltammetry measurements of all complexes
- HOMO/LUMO determination
- Development of a simple model for pre-evaluation of dyes regarding their applicability in DSSCs
- Preparation of the manuscript

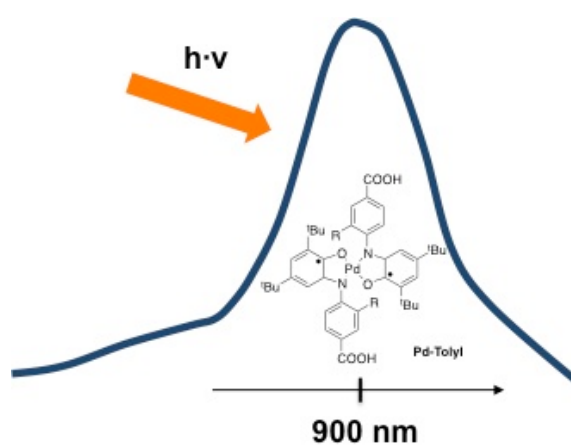


### 3.3 Simple NIR complexes and their applicability in dye-sensitized solar cells

This chapter was published in:

**Authors:** K. Neuthe, C. Popeney\*, K. Bialecka, A. Hinsch, A. Sokolowski, W. Veurmann, R. Haag; *Polyhedron* 2014, 81, 583-587.

<http://dx.doi.org/10.1016/j.poly.2014.07.015>



Author contribution:


- Synthesis and design of NIR ligands and complex **Ni-Prop** based on HOMO/LUMO estimation
- Supervision of Anja Sokolowski working on optimization of ligand synthesis and complex formation of NIR complex **Ni-Prop**
- Cyclic voltammetry measurements of all dyes
- HOMO/LUMO determination
- Preparation of DSSC devices and recording of J/V curves under sunlight illumination
- Preparation of the manuscript

## 4 Summary and conclusion

This work examines new metal-based complexes as dyes for application in dye-sensitized solar cells. The dyes were designed and synthesized to enhance the efficiency of DSSC devices. In general, the strategy was to extend the absorption range of the dyes currently used. Therefore ruthenium dyes with varying extended  $\pi$ -conjugated donor systems and near-infrared absorbing group 10 metal complexes were synthesized. Furthermore, two anchoring systems for the adsorption of the dyes onto different semiconductor materials were investigated. Carboxylate anchors were used for TiO<sub>2</sub> based devices. Phosphonate anchors were examined regarding their applicability on ZnO based DSSC devices.

To extend the absorption range of ruthenium complexes, donor ligands were systematically changed and evaluated with respect to their optical and electrochemical properties. Ligands were altered with respect to the degree of their  $\pi$ -conjugation and hydrophobic character. In addition to the donor ligands, the ratio of the donor and anchor ligands was varied. Extension of the  $\pi$ -conjugation of the donor ligand led to a shift of the absorption maximum to longer wavelengths and to an increase of the extinction coefficient. Changing the hydrophobic character of the ligand had no significant impact on the absorption maximum and extinction coefficient of the metal to ligand charge transfer transition of the dye. Dyes that carried one anchor ligand, a thiocyanate (SCN) donor moiety, and one extended donor ligand showed a broadening of the absorption and an increase of the extinction coefficient in comparison to SCN-free dyes that carried two anchors. Likewise, SCN-containing dyes with an extended,  $\pi$ -conjugated donor ligand lowered the LUMO level of the complexes. The anchor-to-ligand ratio of the dye did not affect the adsorption onto the TiO<sub>2</sub> surface, but the size of the donor ligand did. Introduction of an alkyl substituted donor ligand led to a reduced adsorption of the complex on the TiO<sub>2</sub> surface. Whereas the complex carrying the most extended donor ligand formed aggregates. All dyes were tested in TiO<sub>2</sub> based DSSCs. The efficiency of the cells was mainly affected by the adsorption behavior of the dyes rather than their absorption and electrochemical properties. The SCN-containing complex with the less substituted or extended donor outperformed the other dyes.

Carboxylates are commonly applied anchor systems in TiO<sub>2</sub> based DSSCs. They are, however, detrimental for ZnO based devices as they dissolve the surface. Hence, new ruthenium complexes carrying phosphonate anchor groups were prepared to test their applicability. For



comparison, dye analogs with carboxylate anchor groups were also prepared. Unexpectedly, the efficiency of cells studied with phosphonate-anchored dyes was inferior to those tested with their carboxylic anchored equivalents. This finding could only be partially attributed to the anchor's adsorption behavior on ZnO. One of the main conclusions that could be drawn from this study is that the distance of the LUMO level of the dye to the conducting band of ZnO had a bigger impact on the efficiency of the cell than the adsorption and absorption properties.

In order to cover the near-infrared region of the solar spectrum with DSSCs, symmetric NIR-absorbing nickel diiminosemibenzoquinone and palladium iminosemibenzoquinone complexes were synthesized and tested in TiO<sub>2</sub> based DSSCs. Different electron-withdrawing ligands that affected the energy levels of the dyes were incorporated. However, no correlation between the strength of the electron-withdrawing group and the energy levels was identified. Of all the dyes synthesized, two dyes were successfully applied in prototypical photovoltaic devices using an ionic liquid based electrolyte. They yielded photoconversion efficiency values between 0.21 and 0.35%. We found that the performance of the NIR dyes tested can be improved by increasing their adsorption behavior on TiO<sub>2</sub> and the tolerance of the complexes towards the iodide containing redox mediator that is used in the DSSC electrolyte.

## 5 Outlook

Renewable energy like water, wind, and solar energy has to play a major role in a global answer how to meet the rising energy demand of a growing population. Solar energy should play an important part as it is ubiquitous, free, and can be produced locally. Dye-sensitized solar cells are of special interest as they are theoretically cheaper in production than other photovoltaic technologies and more versatile in their application. For a broad employment of DSSCs in the future energy supply, advances in the fundamental knowledge of the underlying processes have to be gained and implemented. Being able to harvest light from the entire solar spectrum would lead to more efficient DSSC devices. However, even dyes with broad absorption from the UV/Vis to the NIR region usually have low IPCE values at long wavelengths. This observation indicates there is only weak contribution to the photocurrent from this region. Thus, instead of trying to design and use a single panchromatic or solar matched sensitizer, a combination of different dyes in one device should be pursued. One of the established ruthenium dyes should cover the absorption range of 300-600 nm. A coadsorbed NIR dye should ensure efficient light harvesting at longer wavelengths. Group 10 metal dyes are potential candidates to cover the NIR region. Improvements have yet to be made concerning anchoring of the dyes and their energy levels. The synthesis of ruthenium and NIR dyes has to be improved in terms of yields and scale in order to establish continuous syntheses using reactors and ensure cheap production. It is important to gain further insights on the loss reactions in DSSCs and how they can be avoided with the right electrolyte. Furthermore, finding alternative redox-mediators and solvents will increase the maximum  $V_{OC}$  and increase the stability of the dye.



## 6 Zusammenfassung

Im Rahmen der Arbeit wurden neue Farbstoffe für die Anwendung in farbstoffsensibilisierten Solarzellen (FSZ) entworfen, hergestellt und charakterisiert. Ziel war es dabei Farbstoffe zu erhalten, die dazu beitragen die Effizienz von FSZ zu erhöhen. Dies sollte mit Farbstoffen erreicht werden, deren Absorptionsmaxima im langwelligen Bereich des Sonnenspektrums liegen, so dass der spektrale Nutzungsbereich der Solarzelle erweitert wird. Der Fokus lag dabei auf der Entwicklung neuer Liganden für Ruthenium-Farbstoffe sowie neuer Übergangsmetallkomplexe, die dafür bekannt sind, Sonnenlicht im infrarotnahen Bereich zu absorbieren. Zusätzlich wurden zwei Ankersysteme für die Adsorption der Farbstoffe auf unterschiedlichen Halbleitermaterialien untersucht. Carbonsäurebasierte Anker wurden für TiO<sub>2</sub> basierte FSZ verwendet, phosphonsäurebasierte Anker wurden hinsichtlich ihrer Eignung für die Anwendung in ZnO-basierten FSZ untersucht.

Die Komplexe wurden zunächst nach teilweise literaturbekannten Methoden hergestellt und massenspektrometrisch sowie NMR-spektroskopisch charakterisiert. Zur Beurteilung der Eignung für die Anwendung in FSZ wurden die hergestellten Komplexe im Anschluss mit UV/Vis- und Fluoreszenzspektroskopie sowie elektrochemischen Methoden untersucht. Zu den elektrochemischen Methoden zählen sowohl die Cyclovoltammetrie an Platinelektroden als auch Anwendungstests in Farbstoffsolarzellen.

Zur Einstellung der gewünschten Absorptionseigenschaften wurden die Donorliganden heteroleptischer, thiocyanathaltiger und -freier Ruthenium(II)komplexe systematisch variiert. Die Liganden wurden hinsichtlich ihrer hydrophoben Eigenschaften und der Ausdehnung ihres  $\pi$ -Systems modifiziert. Die Farbstoffe variierten außerdem hinsichtlich des Verhältnisses von Anker- und Donorliganden. Die Erweiterung der  $\pi$ -Konjugation der Liganden führte zu einer Verschiebung des Absorptionsmaximums der Komplexe zu Bereichen höherer Wellenlänge und zu einer Erhöhung des Extinktionskoeffizienten. Farbstoffe mit einer Ankergruppe, einer Thiocyanat-Donorgruppe und einem erweiterten Donorliganden zeigten eine Verbreiterung der Absorption und einen größeren Extinktionskoeffizienten als thiocyanatfreie Farbstoffe mit zwei Ankergruppen und einem erweiterten Donorliganden. Bei thiocyanathaltigen Farbstoffen, die mit erweiterten  $\pi$ -Systemen substituiert wurden, konnte zudem eine Verringerung der Energie des niedrigsten unbesetzten Molekülorbitals (LUMO) beobachtet werden. Im Gegensatz zur Größe des Donorliganden hatte das Anker-zu-Donor-

Verhältnis keinen signifikanten Einfluss auf die Adsorption der Farbstoffe an TiO<sub>2</sub>. Die Einführung eines Alkylsubstituenten verringerte die Adsorption, während der Komplex mit dem ausgedehntesten  $\pi$ -System Aggregate auf der Halbleiteroberfläche bildete.

Alle Farbstoffe wurden in TiO<sub>2</sub>-basierten FSZ getestet. Die Effizienz der Zellen wurde dabei im größeren Maß von der Adsorption der Farbstoffe als von deren Absorptions- und elektrochemischen Eigenschaften beeinflusst. Die höchste Effizienz wurde mit einem thiocyanathaltigem Farbstoff mit nur gering ausgedehntem  $\pi$ -System gemessen.

Zur Verankerung der Farbstoffe auf TiO<sub>2</sub>-basierten FSZ werden gewöhnlich Carbonsäuren verwendet. In ZnO-basierten FZO können diese Anker allerdings zu einer Auflösung der ZnO-Oberfläche führen. Es wurden daher Rutheniumkomplexe mit Phosphonat- und Carbonsäureankern hergestellt und hinsichtlich ihrer Eignung verglichen. Anders als angenommen wurde gezeigt, dass Phosphonate als Anker für ZnO den Carboxylatankern nicht überlegen ist. Dieser Fund konnte allerdings nur teilweise dem Adsorptionsverhalten zugeschrieben werden. Es wurde ermittelt, dass ein Zusammenhang zwischen dem Wirkungsgrad der Zelle, d.h. der Leistung des Komplexes und dem Abstand des LUMOs des Farbstoffes vom Leitungsband von ZnO besteht. Dieser Abstand hatte einen größeren Einfluss auf die Effizienz der FSZ als die Absorptions- und Adsorptionseigenschaften der Farbstoffe.

Für die Abdeckung des nahen Infrarotbereichs des Sonnenspektrum mit FSZ wurden symmetrische Nickel(II)- und Palladium(II)-(Di)iminosemichinonate hergestellt und in TiO<sub>2</sub>-basierten FSZ getestet. Verschiedene elektronenziehende Substituenten, welche die Energieniveaus der Farbstoffe beeinflussten, wurden integriert. Es konnte kein Zusammenhang zwischen der Stärke des elektronenziehenden Substituenten und der Lage des Energieniveaus festgestellt werden. Zwei der hergestellten Farbstoffe wurden erfolgreich in einfachen FSZ eingesetzt. Sie erreichten Effizienzen von 0.21 und 0.35%. Die Effizienz des Nickelfarbstoffes war dabei höher als bekannte Werte von Nickelfarbstoffen, die keine Nahinfrarotabsorber sind. Wir haben festgestellt, dass die Leistungsfähigkeit der Nickel- und Palladiumfarbstoffe durch Verbesserung ihres Adsorptionsverhaltens auf TiO<sub>2</sub> und ihrer Stabilität gegenüber dem iodidhaltigen Redoxmediator erhöht werden kann.

## 6. References

1. Administration, U. S. E. I. International Energy Outlook 2013. <http://www.eia.gov/forecasts/ieo/index.cfm> 1–312 (2013).
2. Umweltbundesamt. (Bundesministerium für Umwelt, Naturschutz und Reaktorsicherheit). at <<http://www.umweltbundesamt.de/daten/klimawandel/atmosphaerische-treibhausgas-konzentrationen>>
3. Deffeyes, K. S. *Beyond Oil: The View from Hubbert's Peak*. (Hill and Wang, 2005).
4. Hirsch, L. R. The Inevitable Peaking of World Oil Production. *The Atlantic Council of the United States* XVI, 1–10 (2005).
5. Henning, H.-M. & Palzer, A. studie-energiesystem-deutschland-2050. *Fraunhofer Institut für Solare Energiesysteme* 1–46 (2013).
6. NREL, R. G. 2011 Renewable Energy Data Book (Revised) (Book), Energy Efficiency & Renewable Energy (EERE). *U.S. Department of Energy* 1–128 (2012).
7. Erneuerbare Energien in Zahlen. *Bundesministerium für umwelt, Naturschutz und reaktorsicherheit (Bmu)* 1–112 (2013).
8. Lewis, N. S. Toward Cost-Effective Solar Energy Use. *Science* 315, 798–801 (2007).
9. Burger, P. D. B. Stromproduktion aus Solar- und Windenergie 2013. *Fraunhofer Institut für Solare Energiesysteme* 1–263 (2014).
10. Zhang, S., Yang, X., Numata, Y. & Han, L. Highly efficient dye-sensitized solar cells: progress and future challenges. *Energy Environ. Sci.* 6, 1443 (2013).
11. Ma, W., Jiao, Y. & Meng, S. Predicting Energy Conversion Efficiency of Dye Solar Cells from First Principles. *J. Phys. Chem. C* 140116143326007 (2014). doi:10.1021/jp410982e
12. Hagfeldt, A., Boschloo, G., Sun, L., Kloo, L. & Pettersson, H. Dye-sensitized solar cells. *Chem. Rev.* 110, 6595–6663 (2010).
13. O'Regan, B. & Grätzel, M. A low-cost, high-efficiency solar cell based on dye-sensitized colloidal TiO<sub>2</sub> films. *Nature* 353, 737–739 (1991).
14. Nazeeruddin, M. K. *et al.* Acid–Base Equilibria of (2,2'-Bipyridyl-4,4'-dicarboxylic acid)ruthenium(II) Complexes and the Effect of Protonation on Charge-Transfer Sensitization of Nanocrystalline Titania. *Inorg. Chem.* 38, 6298–6305 (1999).
15. Grätzel, M. Recent advances in sensitized mesoscopic solar cells. *Acc. Chem. Res.* 42, 1788–1798 (2009).
16. Péchy, P. *et al.* Engineering of Efficient Panchromatic Sensitizers for Nanocrystalline TiO<sub>2</sub>-Based Solar Cells. *J. Am. Chem. Soc.* 123, 1613–1624 (2001).
17. Bernardi, M. & Grossman, J. C. Optimal Sunlight Harvesting in Photovoltaics and Photosynthesis. *J. Phys. Chem. C* 117, 26896–26904 (2013).
18. Zakeeruddin, S. M. *et al.* Design, Synthesis, and Application of Amphiphilic Ruthenium Polypyridyl Photosensitizers in Solar Cells Based on Nanocrystalline TiO<sub>2</sub> Films. *Langmuir* 18, 952–954 (2002).
19. Wang, P. *et al.* A stable quasi-solid-state dye-sensitized solar cell with an amphiphilic ruthenium sensitizer and polymer gel electrolyte. *Nat Mater* 2, 402–407 (2003).
20. Jiang, K.-J., Masaki, N., Xia, J.-B., Noda, S. & Yanagida, S. A novel ruthenium sensitizer with a hydrophobic 2-thiophen-2-yl-vinyl-conjugated bipyridyl ligand for effective dye sensitized TiO<sub>2</sub> solar cells. *Chem. Commun.* 2460 (2006).

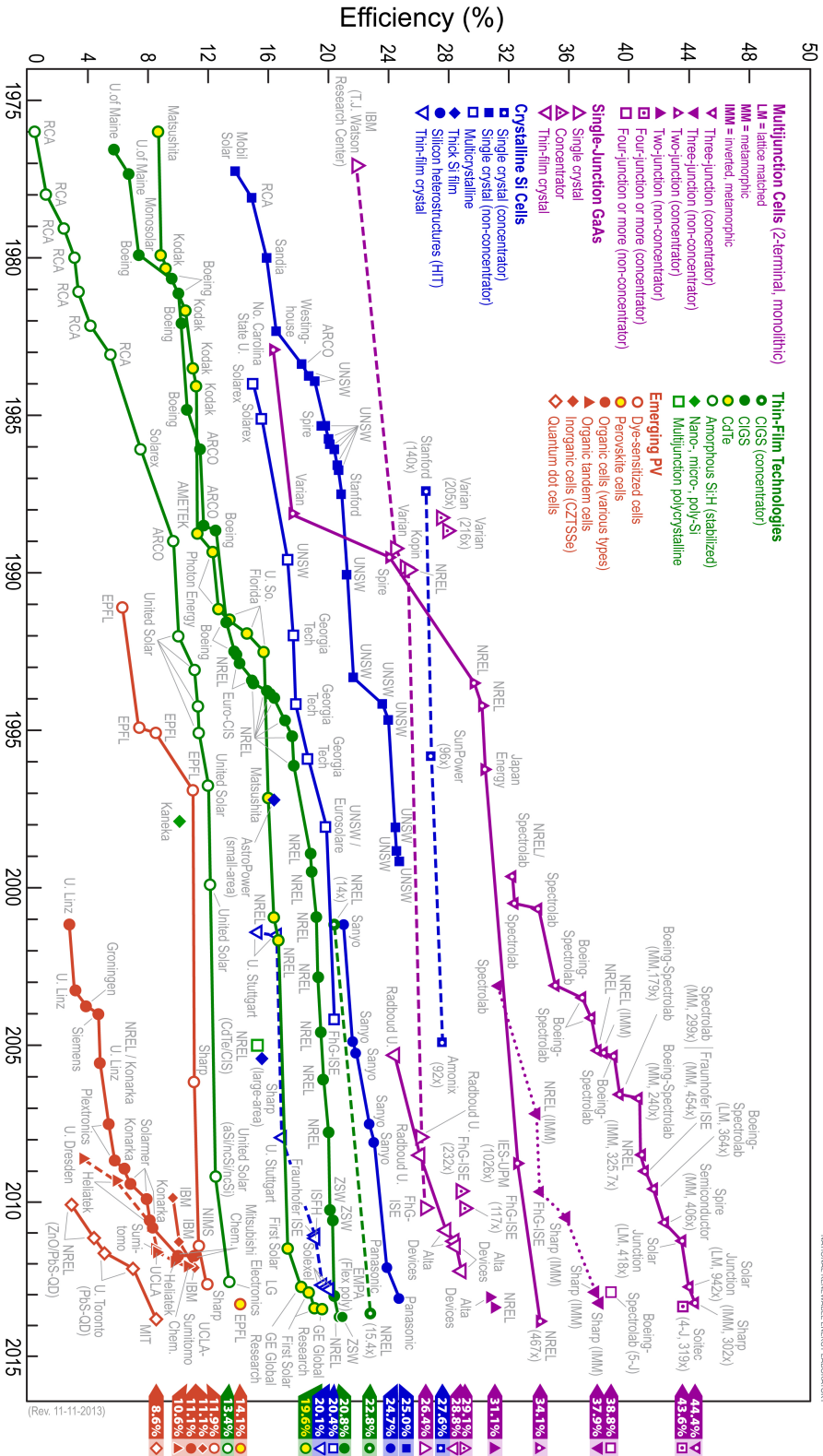


- doi:10.1039/b602989b
21. Wang, P., Klein, C., Humphry-Baker, R., Zakeeruddin, S. M. & Grätzel, M. A High Molar Extinction Coefficient Sensitizer for Stable Dye-Sensitized Solar Cells. *J. Am. Chem. Soc.* **127**, 808–809 (2005).
  22. Suresh, T. *et al.* Novel ruthenium sensitizer with multiple butadiene equivalent thienyls as conjugation on ancillary ligand for dye-sensitized solar cells. *ORGANIC ELECTRONICS* 1–6 (2013). doi:10.1016/j.orgel.2013.04.048
  23. Yin, J.-F., Velayudham, M., Bhattacharya, D., Lin, H.-C. & Lu, K.-L. Structure optimization of ruthenium photosensitizers for efficient dye-sensitized solar cells – A goal toward a ‘bright’ future. *Coordination Chemistry Reviews* **256**, 3008–3035 (2012).
  24. Yum, J.-H. *et al.* High efficient donor-acceptor ruthenium complex for dye-sensitized solar cell applications. *Energy & Environmental Science* **2**, 100–102 (2009).
  25. Kim, J.-J. & Yoon, J. A new ruthenium sensitizer containing dipyrindylamine ligand for effective nanocrystalline dye-sensitized solar cells. *Inorganica Chimica Acta* **394**, 506–511 (2013).
  26. Yin, J.-F. *et al.* Toward Optimization of Oligothiophene Antennas: New Ruthenium Sensitizers with Excellent Performance for Dye-Sensitized Solar Cells. *Chem. Mater.* **22**, 4392–4399 (2010).
  27. Chou, C.-C. *et al.* Ruthenium(II) Sensitizers with Heteroleptic Tridentate Chelates for Dye-Sensitized Solar Cells. *Angew. Chem. Int. Ed.* **50**, 2054–2058 (2011).
  28. Funaki, T., Onozawa-Komatsuzaki, N., Kasuga, K., Sayama, K. & Sugihara, H. New class of thiocyanate-free cyclometalated ruthenium(II) complexes having a pyridylquinoline derivative for near-infrared sensitization of dye-sensitized solar cells. *INORGANIC CHEMISTRY COMMUNICATIONS* **35**, 281–283 (2013).
  29. Bessho, T. *et al.* New Paradigm in Molecular Engineering of Sensitizers for Solar Cell Applications. *J. Am. Chem. Soc.* **131**, 5930–5934 (2009).
  30. Nguyen, H. T., Ta, H. M. & Lund, T. Thermal thiocyanate ligand substitution kinetics of the solar cell dye N719 by acetonitrile, 3-methoxypropionitrile, and 4-tert-butylpyridine. *Solar Energy Materials and Solar Cells* **91**, 1934–1942 (2007).
  31. Hsu, Y.-C., Zheng, H., T'suen Lin, J. & Ho, K.-C. On the structural variations of Ru(II) complexes for dye-sensitized solar cells. *Solar Energy Materials and Solar Cells* **87**, 357–367 (2005).
  32. Klein, C. *et al.* Engineering of a Novel Ruthenium Sensitizer and Its Application in Dye-Sensitized Solar Cells for Conversion of Sunlight into Electricity. *Inorg. Chem.* **44**, 178–180 (2005).
  33. Mishra, A. *et al.* A Thiophene-Based Anchoring Ligand and Its Heteroleptic Ru(II)-Complex for Efficient Thin-Film Dye-Sensitized Solar Cells. *Adv. Funct. Mater.* **21**, 963–970 (2011).
  34. Sauv e, G. *et al.* High Quantum Yield Sensitization of Nanocrystalline Titanium Dioxide Photoelectrodes with cis-Dicyanobis(4,4'-dicarboxy-2,2'-bipyridine)osmium(II) or Tris(4,4'-dicarboxy-2,2'-bipyridine)osmium(II) Complexes. *J. Phys. Chem. B* **104**, 3488–3491 (2000).
  35. Bessho, T. *et al.* An element of surprise—efficient copper-functionalized dye-sensitized solar cells. *Chem. Commun.* 3717 (2008). doi:10.1039/b808491b
  36. Linfoot, C. L. *et al.* A nickel-complex sensitizer for Dye-Sensitized Solar Cells. *Solar Energy* **85**, 1195–1203 (2011).
  37. Islam, A. *et al.* Dye Sensitization of Nanocrystalline Titanium Dioxide with Square Planar Platinum(II) Diimine Dithiolate Complexes. *Inorg. Chem.* **40**, 5371–5380

- (2001).
38. Geary, E. A. M. *et al.* Synthesis, structure and properties of [Pt(2,2'-bipyridyl-5,5'-dicarboxylic acid)(3,4-toluenedithiolate)]: tuning molecular properties for application in dye-sensitized solar cells. *Dalton Trans.* 3757 (2003). doi:10.1039/b306241d
  39. Geary, E. A. M. *et al.* Synthesis, Structure, and Properties of [Pt(II)(diimine)(dithiolate)] Dyes with 3,3', 4,4', and 5,5'-Disubstituted Bipyridyl: Applications in Dye-Sensitized Solar Cells. *Inorg. Chem.* **44**, 242–250 (2005).
  40. Geary, E. A. M. *et al.* Spectroscopic, electrochemical and computational study of Pt–diimine–dithiolene complexes: rationalising the properties of solar cell dyes. *Dalton Trans.* 3701 (2008). doi:10.1039/b719789f
  41. Aragoni, C. M. *et al.* Photoinduced conductivity and nonlinear optical properties of [M(R,R'-timdt)<sub>2</sub>] dithiolenes (M = Ni, Pd, Pt; R,R'-timdt = monoreduced imidazolidine-2,4,5-trithione) as materials for optically driven switches and photodetectors. *INORGANIC CHEMISTRY COMMUNICATIONS* 869–872 (2002).
  42. Ito, S. *et al.* High-Efficiency Organic-Dye-Sensitized Solar Cells Controlled by Nanocrystalline-TiO<sub>2</sub> Electrode Thickness. *Adv. Mater.* **18**, 1202–1205 (2006).
  43. Geiger, T. *et al.* Molecular Design of Unsymmetrical Squaraine Dyes for High Efficiency Conversion of Low Energy Photons into Electrons Using TiO<sub>2</sub> Nanocrystalline Films. *Adv. Funct. Mater.* **19**, 2720–2727 (2009).
  44. Mishra, A., Fischer, M. K. R. & Bäuerle, P. Metallfreie organische Farbstoffe für farbstoffsensibilisierte Solarzellen - von Struktur-Eigenschafts-Beziehungen zu Designregeln. *Angew. Chem.* **121**, 2510–2536 (2009).
  45. Karthikeyan, C. S., Peter, K. & Wietasch, H. Highly efficient solid-state dye-sensitized TiO<sub>2</sub> solar cells via control of retardation of recombination using novel donor-antenna dyes. *Solar energy materials ...* (2007). doi:10.1016/j.solmat.2006.10.006
  46. Ito, S. *et al.* High-conversion-efficiency organic dye-sensitized solar cells with a novel indoline dye. *Chem. Commun.* **0**, 5194–5196 (2008).
  47. Wang, P. *et al.* Stable New Sensitizer with Improved Light Harvesting for Nanocrystalline Dye-Sensitized Solar Cells. *Adv. Mater.* **16**, 1806–1811 (2004).
  48. Hara, K. *et al.* Dye-sensitized nanocrystalline TiO<sub>2</sub> solar cells based on novel coumarin dyes. *Solar Energy Materials and Solar Cells* **77**, 89–103 (2003).
  49. Deubel, D. V. & Ziegler, T. DFT Study of Olefin versus Nitrogen Bonding in the Coordination of Nitrogen-Containing Polar Monomers to Diimine and Salicylaldiminato Nickel(II) and Palladium(II) Complexes. Implications for Copolymerization of Olefins with Nitrogen-Containing Polar Monomers. *Organometallics* **21**, 1603–1611 (2002).
  50. Wang, C. *et al.* Neutral Nickel(II)-Based Catalysts for Ethylene Polymerization. *Organometallics* **17**, 3149–3151 (1998).
  51. Chaudhuri, P. *et al.* Electronic Structure of Bis( o-iminobenzosemiquinonato)metal Complexes (Cu, Ni, Pd). The Art of Establishing Physical Oxidation States in Transition-Metal Complexes Containing Radical Ligands. *J. Am. Chem. Soc.* **123**, 2213–2223 (2001).

# 7. Appendix

## a. Figures



A. 1 Best research-cell efficiencies.

## 8. Curriculum vitae

Der Lebenslauf ist in der Online-Version aus Gründen des Datenschutzes nicht enthalten



Der Lebenslauf ist in der Online-Version aus Gründen des Datenschutzes nicht enthalten

Der Lebenslauf ist in der Online-Version aus Gründen des Datenschutzes nicht enthalten